Power-Hardware-in-the-Loop Experiments of a Microgrid With a Grid-Forming Battery Inverter

Preprint

Annabelle Pratt, Kumaraguru Prabakar, and Martha Symko-Davies

National Renewable Energy Laboratory

Presented at the 2025 IEEE Power and Energy Society General Meeting
Austin, Texas
July 27–31, 2025

NREL is a national laboratory of the U.S. Department of Energy
Office of Energy Efficiency & Renewable Energy
Operated under Contract No. DE-AC36-08GO28308

This report is available at no cost from NREL at www.nrel.gov/publications.

Conference Paper
NREL/CP-5D00-91813
November 2025

Power-Hardware-in-the-Loop Experiments of a Microgrid With a Grid-Forming Battery Inverter

Preprint

Annabelle Pratt, Kumaraguru Prabakar, and Martha Symko-Davies

National Renewable Energy Laboratory

Suggested Citation
Pratt, Annabelle, Kumaraguru Prabakar, and Martha Symko-Davies. 2025. *Power-Hardware-in-the-Loop Experiments of a Microgrid With a Grid-Forming Battery Inverter: Preprint*. Golden, CO: National Renewable Energy Laboratory. NREL/CP-5D00-91813. https://www.nrel.gov/docs/fy26osti/91813.pdf.

NREL is a national laboratory of the U.S. Department of Energy
Office of Energy Efficiency & Renewable Energy
Operated under Contract No. DE-AC36-08GO28308

This report is available at no cost from NREL at www.nrel.gov/publications.

Conference Paper
NREL/CP-5D00-91813
November 2025

15013 Denver West Parkway
Golden, CO 80401
303-275-3000 • www.nrel.gov

NOTICE

This work was authored in part by NREL for the U.S. Department of Energy (DOE), operated under Contract No. DE-AC36-08GO28308. Funding provided by U.S. Department of Energy Office of Energy Efficiency and Renewable Energy Solar Energy Technologies Office and Hydrogen and Fuel Cell Technologies Office. The views expressed herein do not necessarily represent the views of the DOE or the U.S. Government. The U.S. Government retains and the publisher, by accepting the article for publication, acknowledges that the U.S. Government retains a nonexclusive, paid-up, irrevocable, worldwide license to publish or reproduce the published form of this work, or allow others to do so, for U.S. Government purposes.

Cover photos (clockwise from left): Josh Bauer, NREL 61725; Visualization from the NREL Insight Center; Getty-181828180; Agata Bogucka, NREL 91683; Dennis Schroeder, NREL 51331; Werner Slocum, NREL 67842.

Power-Hardware-in-the-Loop Experiments of a Microgrid With a Grid-Forming Battery Inverter

Annabelle Pratt, Kumaraguru Prabakar, Martha Symko-Davies
Power Systems Engineering Center
National Renewable Energy Laboratory
Golden, Colorado, USA
annabelle.pratt@nrel.gov

***Abstract*—Microgrids continue to be deployed at various scales, and they are transitioning away from using conventional generating resources to increasingly relying on inverter-based resources (IBRs) as the voltage and frequency leaders. At the San Diego Gas & Electric Company Borrego Springs Microgrid, a battery inverter was upgraded with grid-forming (GFM) capability to serve as the island leader. Hardware-in-the-loop (HIL) experiments were conducted to de-risk the field deployment. This paper presents the HIL experimental results from an HIL test bed that uses a power-hardware-in-the-loop (PHIL) interface with a power inductor that was previously developed for PHIL simulations of microgrids where the inverters need to switch modes, i.e., between grid-following and GFM as the microgrid transitions between grid-connected and islanded operation. This paper presents more details on the interface and HIL simulation results of planned islanding and load steps in islanded operation to show the effectiveness of the inverters in managing the voltage and frequency.**

***Index Terms*-- Battery energy storage system, controller hardware-in-the-loop, grid-forming inverter, hardware-in-the-loop, microgrids, power-hardware-in-the-loop.**

I. INTRODUCTION

A microgrid, according to the U.S. Department of Energy (DOE), is able to separate from the main grid, or island, and therefore it requires generation resources to supply all (or at least all critical) microgrid loads, a switch that can disconnect the microgrid from the main grid, and a source that defines the voltage and frequency of the system [1]. Traditionally, this requirement has been fulfilled by either natural gas or diesel generators, but there is increased interest in using inverter-based renewable sources, such as stationary battery energy storage systems (BESS) or fuel cells with grid-forming (GFM) inverters [2], [3].

San Diego Gas & Electric Company (SDG&E) established the multi-megawatt Borrego Springs Microgrid [4] in Borrego Springs, California, to improve resilience for this remote, disadvantaged desert community with increased outage risks related to extreme climate conditions, including high temperatures, thunderstorms, monsoon flooding, and high winds. The community is at the end of a single radial overhead transmission line with a high proportion of photovoltaic (PV) generation. It has multiple critical and priority loads related to emergency, municipal, and health services, in addition to large agricultural loads for pumping water. Unplanned and planned substation and transmission maintenance outages ranged from 4 h to more than 20 h during the past decade.

Historically, microgrids have relied on conventional diesel generators as the GFM resources for black starts, islanding, frequency stabilization, and primary energy capacity, with BESS providing grid-following (GFL) support. Through a project funded by DOE's Solar Energy Technologies Office and led by SDG&E, the island leader role was transitioned to a GFM battery inverter through hardware upgrades and a new microgrid controller. The project aims to evaluate the frequency response behavior of the microgrid with an inverter-based resource (IBR) serving as island leader under practical operating conditions. A second project, funded by DOE's Hydrogen and Fuel Cell Technologies Office and led by NREL, in partnership with SoCalGas, will identify recommendations for interconnection and interoperability of grid-forming fuel cell inverters targeting community microgrids. NREL is performing the PHIL simulations for both projects.

The deployment of state-of-the-art renewable distributed energy resources (DERs) and control strategies in utility grids and microgrids must be undertaken carefully with stepwise validation to mitigate risks of customer service disruptions. Hardware-in-the-loop (HIL) simulations can de-risk microgrid deployments and provide early insights by testing conditions not yet demonstrated during field operations [3]. SDG&E is employing HIL simulations of the Borrego Springs Microgrid at the National Renewable Energy Laboratory's (NREL's)

This work was authored by the National Renewable Energy Laboratory, operated by Alliance for Sustainable Energy, LLC, for the U.S. Department of Energy (DOE) under Contract No. DE-AC36-08GO28308. Funding provided by U.S. Department of Energy Office of Energy Efficiency and Renewable Energy Solar Energy Technologies Office and Hydrogen and Fuel Cell Technologies Office. The views expressed in the article do not necessarily represent the views of the DOE or the U.S. Government. The U.S. Government retains and the publisher, by accepting the article for publication, acknowledges that the U.S. Government retains a nonexclusive, paid-up, irrevocable, worldwide license to publish or reproduce the published form of this work, or allow others to do so, for U.S. Government purposes.

Energy Systems Integration Facility (ESIF) to build confidence that the microgrid can be formed by an IBR and is stable. This paper presents the results from HIL experiments of the SDG&E Borrego Springs Microgrid operating with 100% renewable generation to inform the wider industry of key outcomes to date. Section II provides an overview of the microgrid, Section III describes the HIL test bed with power-hardware-in-the-loop (PHIL) and controller-hardware-in-the-loop (CHIL) interfaces, Section IV presents the HIL simulation results, and Section V concludes and discusses future work.

II. Borrego Springs Microgrid Description

The Borrego Springs community is served by three 12-kV distribution circuits. The distribution grid has a net peak load of 12 MW [5] and contains approximately 15 MW of PV generation, including approximately 8.6 MW of non-dispatchable, non-controllable customer rooftop PV generation. A 26-MW_{ac} PV plant is connected to the 69-kV bus, and a 6.3 MW_{ac} concentrating PV plant is connected to a 12-kV circuit. Presently, these PV plants are unavailable during microgrid operations. Figure 1 shows the DERs in the microgrid.

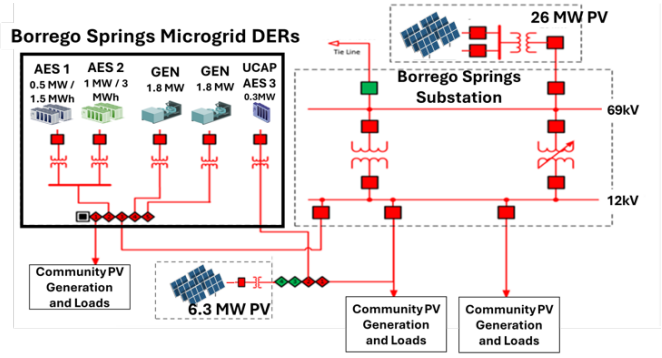

Figure 1. Diagram of the Borrego Springs Microgrid.

The microgrid has historically used two 1.8-MW diesel generators as the voltage and frequency leaders in islanded mode [6], and two GFL utility-scale BESS, rated at 1 MW/3 MWh (AES 2) and 0.5 MW/1.5 MWh (AES 1), respectively. SDG&E aims to operate the Borrego Springs Microgrid in islanded mode either without diesel generators (when the BESS can meet the net load) or with the generators in load-following mode (when their capacity is needed to meet the net load). To achieve this, the 1-MW BESS, AES 2, was upgraded with a GFM inverter that operates as the voltage and frequency leader when the microgrid is islanded and that is operated in GFL mode when the microgrid is grid-connected. The 0.5-MW BESS inverter is always operated in GFL mode. The microgrid also has an ultracapacitor (UCAP) system, AES 3 (0.3 MW/30 s), that operates in GFL mode with a frequency-watt curve. A PXiSE Energy Solutions microgrid controller was implemented to command the assets and provide a visual real-time status of the energy storage systems and other microgrid assets.

III. PHIL Experimental Setup

The diagram in Figure 2 shows the HIL test bed at NREL's ESIF. The setup expands upon an earlier test bed that was developed for the Borrego Springs Microgrid with diesel generators and GFL inverters [5][6].

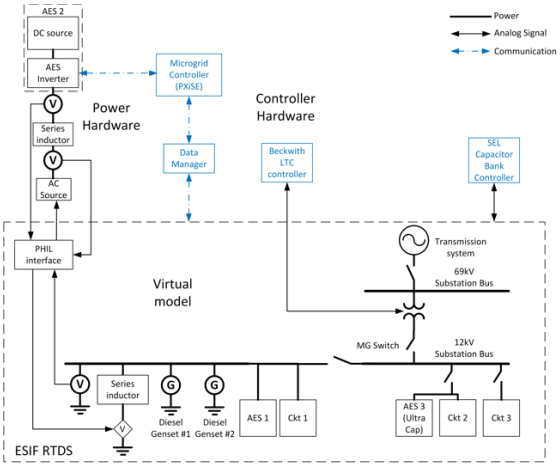

Figure 2. Diagram of the HIL test bed.

The distribution system is simulated in an RTDS Simulator with the time step set to 95 usec. SDG&E provided the model to NREL in the RTDS proprietary simulation software format, RSCAD, and NREL made the necessary modifications to integrate it with the controller and power hardware. The power system model includes a simple representation of the transmission system; the microgrid (MG) switch; the three distribution feeders (Ckt 1, Ckt 2, and Ckt 3), all of which include rooftop PV systems; the two diesel generators, AES 1 and AES 3 on Ckt 2; and interfaces to the hardware. The transmission- and distribution-connected PV plants are not presently configured to be used during microgrid operations and were not included in the RSCAD model. Two load tap changer (LTC) controllers, one capacitor bank controller, and the same microgrid controller that is deployed in the field are interfaced with the RTDS as CHIL.

GFM inverter technology is rapidly advancing, and inverter performance is far from uniform across products, especially in how inverters respond to transitions between grid-connected and islanded operation; therefore AES 2 was implemented as PHIL using a GFM battery inverter from the same manufacturer and line of products as the inverters installed in the Borrego Springs Microgrid and with the same controls. It was interfaced with the RTDS through a controllable AC source in series with an inductor and connected to a controllable DC source that supplies DC power to the inverter, as described in [7].

Figure 3 shows the experimental setup in NREL's ESIF. The CE+T inverter between the AC source and inverter is not used in this setup. Two custom-built measurement boxes with voltage and current transducers can be seen on the floor with oscilloscopes on top. One box also houses an SEL 751 feeder protection relay with synchronization capabilities to control the simulated microgrid switch. We set the allowable frequency, voltage amplitude, and phase differences to 1 Hz, 2V, and 8 degrees, respectively. The 100-kVA power inductor was manufactured to a specification of 1 mH by CTM Magnetics.

We use a Hitachi ABB PCS100 inverter; 100-kW Regatron TopCon TC.ACS voltage amplifiers for the AC source; and a NH Research 9300 controllable DC source that is set to a fixed DC voltage.

Figure 3. PHIL experimental setup with the inverter on the right, to the left of the large computer screens; the AC source in the center, and the power inductor on the left. *Photo by NREL*

A. PHIL Interface With Voltage Amplifier Method

We integrated the hardware inverter with the power system model using the voltage amplifier method introduced in [8]. This PHIL interface method is required because AES 2 operates in GFM mode when the microgrid is islanded and in GFL mode when the microgrid is grid-connected, and the PHIL interface needs to transition between these two states. By matching the impedance of the series inductor in the simulation, $\boldsymbol{Z_s}$, to the impedance in the experimental setup, $\boldsymbol{Z_h}$—which includes the physical inductor, the cables, and the breaker required by the PHIL interface—the current in the simulation matches the current in the hardware [7]. The simulated current can be scaled up by scaling down the impedance in the simulation, $\boldsymbol{Z_s}$, by the current scale-up factor [8]. We need to scale up the 88-kW hardware inverter to represent a 1-MW inverter to match the power rating of AES 2, so out scale-up factor, K, is 11.36, and $\boldsymbol{Z_s} = \boldsymbol{Z_h}/K$.

B. Inductor Value Calculation

We calculated the impedance $\boldsymbol{Z_h}$ using measurements of the voltages at the output of inverter, $\boldsymbol{V_i}$, and at the output of the amplifier, $\boldsymbol{V_g}$, and the current, $\boldsymbol{I_o}$, through the power inductor, as follows: $\boldsymbol{Z_h} = (\boldsymbol{V_i} - \boldsymbol{V_g})/\boldsymbol{I_o} = \Delta\boldsymbol{V}/\boldsymbol{I_o}$.

The vector diagram in Figure 4 shows the voltages and current with their respective phase relationships. We used a Yokogawa WT1806E power analyzer to obtain the per-phase amplitudes of the voltages and current and the phase angle between $\boldsymbol{V_i}$ and $\boldsymbol{I_o}$, denoted as γ, and between $\boldsymbol{V_g}$ and $\boldsymbol{I_o}$, denoted as φ. We then calculate $\boldsymbol{Z_h}$ for each phase, assuming $\boldsymbol{V_g} = V_g + j0$, through the following steps: First, we calculate $\delta = \gamma - \varphi$, then use those values to calculate:

- $\boldsymbol{Vi} = Vi.\cos(\delta) + \mathrm{j}\ Vi.\sin(\delta)$ and
- $\boldsymbol{I_o} = I_o.\cos(\varphi) + \mathrm{j}\ I_o.\sin(\varphi)$.

The voltage drop across inductor can be expressed as:

- $\Delta\boldsymbol{V} = \boldsymbol{Vi} - \boldsymbol{Vg} = (Vi.\cos(\delta) - Vg) + \mathrm{j}Vi.\sin(\delta)$.

From inspection of the vector diagram, its amplitude, ΔV, and phase angle, θ, can also be expressed as:

- $\Delta V = \mathrm{sqrt}((V_i.\cos(\delta) - V_g)^2 + (V_i.\sin(\delta)^2))$
- $\theta = \arctan(V_i.\sin(\delta) / (V_i.\cos(\delta) - V_g))$

The amplitude of the impedance $\boldsymbol{Z_h}$ is $Z_h = \Delta V / I_o$, and its phase angle is $(\theta - \varphi)$, so:

- $\boldsymbol{Z_h} = \Delta V / I_o.\cos(\theta - \varphi) + \mathrm{j}\ \Delta V / I_o.\sin(\theta - \varphi)$.

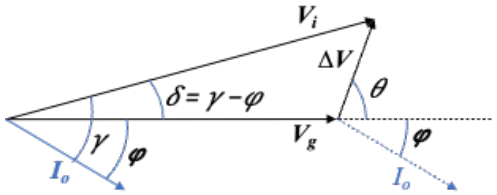

Figure 4. Vector diagram for inductor value calculation.

We took measurements at several power levels and calculated the average inductance and resistance values of $\boldsymbol{Z_h}$. The final values we used for $\boldsymbol{Z_h}$ are 1.3 mH and 75 mohm, based on experimental testing.

Table 1 shows accuracy results for active power, where P_i is the output power of the hardware inverter, P_{sim} is the output power of the equivalent voltage source representing the inverter in the simulation. These results were obtained using the simple microgrid model described in [8]. We achieved an acceptable error at medium to high power, but accuracy deteriorated at lower power. Dynamic accuracy is good as shown in Figure 5 for phase A using results from the planned islanding experiment described in more detail in Section IV.

TABLE I. STEADY-STATE ACCURACY FOR ACTIVE POWER

P_i [kW]	Q_i [kVar]	P_i [%]*	P_{sim}/K	Error [kW]	Error [%]**
7.1	2.3	8	4.78	2.32	33
14.7	2.9	17	13.38	1.32	9
22.4	3.96	25	21.92	0.48	2
30.4	5.49	35	30.11	0.29	1
38.79	7.28	44	38.24	0.55	1
47.36	9.47	54	46.16	1.20	3

* Percentage of hardware inverter power rating ** Percentage of *Pi*

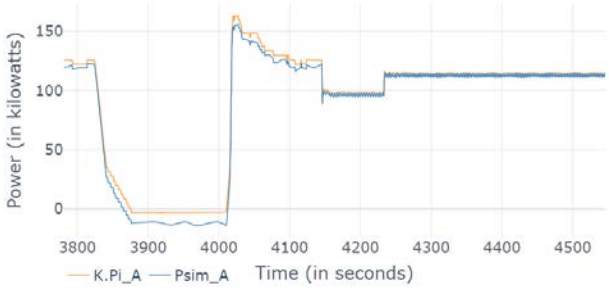

Figure 5. Comparison of scaled hardware and simulated inverter output active power for phase A under dynamic conditions.

IV. EXPERIMENTAL RESULTS

The main purpose of the HIL testing is to evaluate the effectiveness of the inverters in limiting the frequency variability during planned islanding under various operating conditions to improve the likelihood of the formation of a stable microgrid with only renewable, IBRs—i.e., in a low-inertia environment. Planned islanding simulations were performed for different load conditions, including heavy and light load during daytime and nighttime. The simulations were run for at least 3 min of operation after islanding to confirm the stability

of the island. AES 1 is operated in GFL mode, and AES 2 is operated in GFL mode when grid-connected and in GFM mode with droop when islanded. AES 3 operates in GFL mode with a frequency-watt curve. It maintains the state of charge (SOC) of the UCAPs near 90% when it is not actively responding to an under- or overfrequency condition. The diesel generators are used only in heavy load scenarios, in GFL mode, when the renewable resources do not have adequate capacity.

A. Planned Islanding Experimental Results

We performed HIL simulations of a planned islanding event under light load conditions without diesel generators. Part of one feeder within the microgrid was islanded based on the capacity of the available renewable sources (PV and BESS). We used varying load and PV profiles, with a resolution of 1 min, based on historical data from 8–9 a.m. on July 29, 2019.

The project team previously published results [4] with a frequency droop setting of 2% for AES 2 and a frequency-watt curve deadband of either +/- 0.3 Hz or +/- 0.2 Hz for AES 3. This paper presents planned islanding results and results from load steps in islanded operation with updated inverter settings. We used a frequency droop setting of 0.2% and a voltage droop setting of 0.1% for AES 2 and a frequency-watt curve deadband of +/- 0.06 Hz and a maximum output power of 200 kW at 59.408 Hz and 60.592 Hz for AES 3. Further, the RSCAD model of AES 3 used in [4] used frequency measured by a phase-locked loop (PLL) followed by a filter with a time constant of 0.01 s. This technique filtered out fast frequency transients, so AES 3 did not respond. We replaced the frequency input to the UCAP model in this study with the frequency captured from a simulated phasor measurement unit (PMU) to speed up the UCAP response.

Figure 6 shows a planned islanding event and about 3 min of operation after islanding with AES 3. The same results are shown for a shorter time, of about 3 s, in Figure 7. In both figures, the top subplot shows the frequency as captured from a simulated PMU in RSCAD. The bottom subplot shows the output power as recorded by three-phase power meters in RSCAD (AES 1, AES 2, AES 3) and the power flow through the microgrid switch. The microgrid controller reduces the power flow through the microgrid switch to near zero before opening the microgrid isolation switch at 2505 s. It dispatches GLF inverter AES 1 at its full power rating (500 kW), and it dispatches AES 2, which operates in GFL mode while grid-connected, to provide the rest of the net load (340 kW) so that the power flow through the microgrid isolation switch is near zero.

AES 3 periodically charges (at about 20 kW) to maintain its target SOC, then its power drops to zero after it reaches its target SOC. For this experiment, it is charging at 20 kW when the microgrid is islanded. The power flow through the microgrid switch is close to zero at islanding (about 40 kW). The microgrid controller allows islanding if the microgrid switch power flow is below 50 kW. AES 1 output power shows a brief transient. The inverter mode for AES 2 switches from GFL to GFM when the microgrid is islanded, and its output power adjusts to regulate the microgrid voltage and frequency. The frequency drops to 59.89 Hz after islanding, as shown in Figure 6, and then settles at 59.98 Hz.

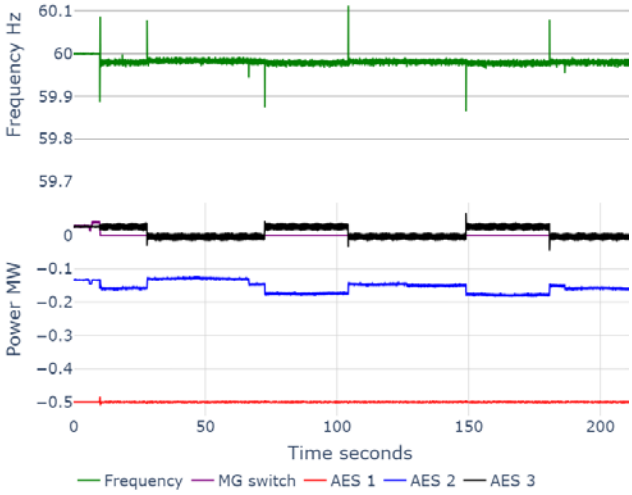

Figure 6. The microgrid frequency (top) and inverter output powers and the power flow through the microgrid switch (bottom) during planned islanding with the ultracapacitor for about 3 min.

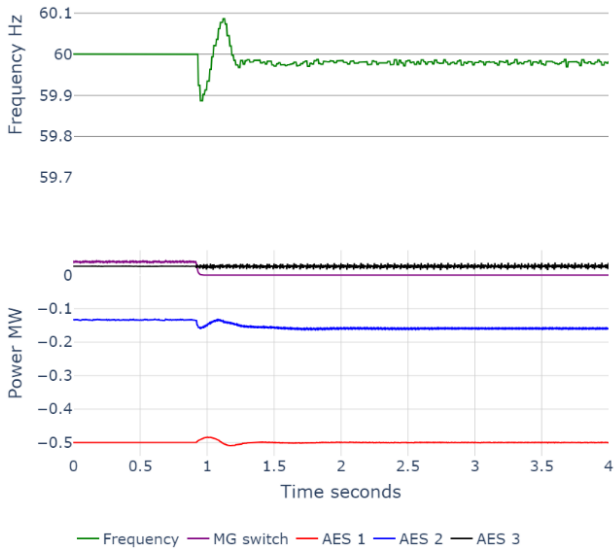

Figure 7. The microgrid frequency (top) and inverter output powers and the power flow through the microgrid switch (bottom) during planned islanding with the ultracapacitor for about 3 s.

We expected AES 3 to respond to a frequency drop to 59.89 Hz by discharging at about 20 kW, based on the frequency-watt curve parameters, but there is no observable response. AES 2 responds almost immediately to stabilize the frequency, so the frequency is below 59.94 Hz for only 75 msec; therefore, the lack of response from AES 3 is believed to be due to the slower dynamic response in the UCAP RSCAD model's controls. The inverter also regulates the voltage well in islanded operation.

There is a frequency transient every time AES 3 starts or stops charging, as shown in Figure 6. AES 3 also does not respond to the frequency transients when it stops and starts charging. The frequency is outside of the frequency envelope deadband for only about 25 msec. We performed two more sets of experiments to further evaluate the frequency response of the inverters, as described in the following two sections.

B. *Experimental Results of Frequency Step Change*

First, we aimed to verify that the AES 3 UCAP model performs as expected. We ran a simulation with the microgrid in grid-connected operation without AES 2, i.e., a software simulation only. We then adjusted the grid frequency to 59.3 Hz in a step change. Figure 8 shows AES 3 power output in the top trace and the input frequency in the bottom trace. AES 3 reaches its maximum output power of 200 kW in 190 msec with the PMU frequency as an input to the UCAP model. We performed the same experiment with the filtered PLL frequency input, and the UCAP reached 200 kW output in 280 msec, so the response is faster with the PMU frequency input; however, the frequency is below 59.94 Hz for only 85 msec during the planned islanding event shown in Figure 7, so it is shorter than the response time with the PMU frequency input.

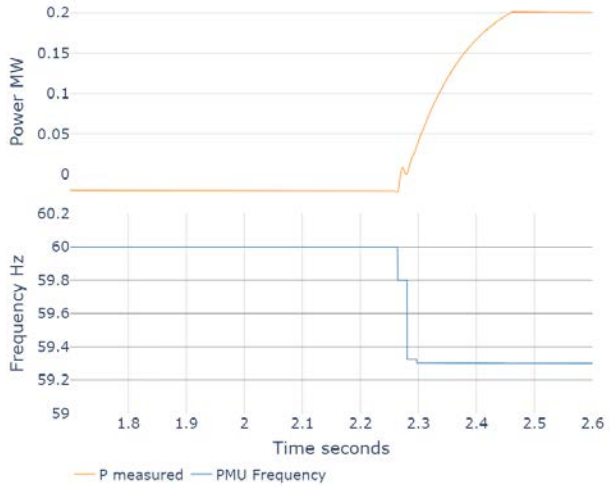

Figure 8. UCAP output power (top, green line) and frequency used as input to UCAP (bottom), captured from a simulated PMU.

C. *Experimental Results of Load Steps*

We simulated load steps in islanded operation because this results in larger frequency variations than during islanding. We used constant loads and PV outputs in the simulation. The starting load is about the same as during the planned islanding experiment. The load is stepped up from 685 kW to 885 kW, i.e., a step-up of 200 kW. The results are shown in Figure 9. The AES 3 output power changes from charging at about 25 kW to discharging, peaking at about 32 kW, when the load is stepped up. The frequency drops as low as 59.58 Hz and is restored above 59.94 Hz within 75 msec; it is above 59.9 Hz by the time AES 3 reaches its maximum discharge rate. The response rates are similar for AES 2 and AES 3, which is to be expected because they use inverters from the same manufacturer and family of products but with different ratings.

The frequency with the PMU measurement input to AES 3 showed significant fluctuations after a load step, so further study is warranted with a filtered PMU measured frequency as an input. The results presented in this paper show that the GFM inverter regulates the frequency quickly and accurately, and that the UCAP, AES 3, contributes when the frequency is outside of its frequency deadband, but does not reach its rated output power because its response time is longer than the dwell time of frequency below the frequency deadband.

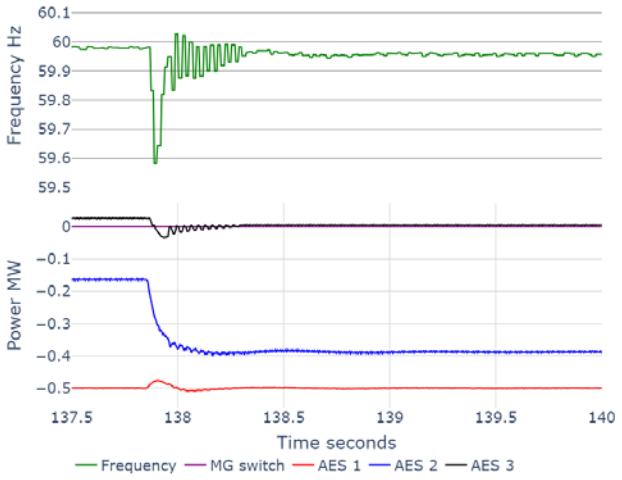

Figure 9. Microgrid frequency (top) and inverter powers (bottom) during a load step of 200 kW in islanded operation with the UCAP.

V. CONCLUSIONS

This paper presents results from HIL experiments of the SDG&E Borrego Springs Microgrid. We use a previously-developed PHIL interface for HIL simulations of microgrids where the inverters need to switch modes, i.e., between GFL and GFM as the microgrid transitions between grid-connected and islanded operation. This paper presents more details on the interface and HIL simulation results of planned islanding and load steps in islanded operation to show the effectiveness of the inverters in managing the microgrid frequency. In the next steps, SDG&E plans to conduct field tests.

ACKNOWLEDGMENT

The authors gratefully acknowledge the leadership of Laurence Abcede and Kim McGrath, principal investigator and project manager for the SETO project at SDG&E, and the support provided by Bob Reedy of DOE. Subhankar Ganguly and Brian Fedish from NREL supported the HIL experiments.

REFERENCES

[1] V. Donde and A. Pratt, "Microgrids as a building block for future grids - topic 4," vol. 4, p. 27, 2022.

[2] Y. Lin, "Research roadmap on grid-forming inverters," 2021.

[3] K. Prabakar, Y. N. Velaga, R. Flores, J. Brouwer, J. Chase, and P. Sen, "Enhancing distribution system resilience using grid-forming fuel cell inverter," in *2022 IEEE Rural Electric Power Conference (REPC)*. IEEE, 2022, pp. 38–42.

[4] L. Abcede, A. Pratt, K. Prabakar and K. McGrath, "Interoperable, Inverter-Based Distributed Energy Resources Enable 100% Renewable and Resilient Utility Microgrids," IEEE Grid Edge Technologies 2025 Conference, Jan. 2025.

[5] K. Prabakar, A. Pratt, et al., "Site-Specific Evaluation of Microgrid Controller Using Controller and Power-Hardware-in-the-Loop," 45th Annual Conference of the IEEE Industrial Electronics Society (IECON), October 2019, Lisbon, Portugal.

[6] J. Wang, A. Pratt, K. Prabakar, B. Miller, and M. Symko-Davies, "Development of an integrated platform for hardware-in-the-loop evaluation of microgrids prior to site commissioning," *Applied Energy*, vol. 290, 2021.

[7] J. Hernandez-Alvidrez *et al.*, "Method to interface grid-forming inverters into power hardware in the loop setups," *47th IEEE Photovoltaic Specialists Conference*, 2020.

[8] A. Pratt, K. Prabakar, S. Ganguly, and S. Tiwari, "Power hardware-in-the-loop interfaces for inverter-based microgrid experiments including transitions," in IEEE ECCE, Oct-Nov 2023, Knoxville, TN.